Spontaneous Aggregation of the Insulin-Derived Steric Zipper Peptide VEALYL Results in Different Aggregation Forms with Common Features

Dirk Matthes[1,†], Venita Daebel[2,†], Karsten Meyenberg[3], Dietmar Riedel[4], Gudrun Heim[4], Ulf Diederichsen[3], Adam Lange[2] and Bert L. de Groot[1]

*1 - **Computational Biomolecular Dynamics Group,** Max Planck Institute for Biophysical Chemistry, Am Fassberg 11, 37077 Göttingen, Germany*
*2 - **NMR-Based Structural Biology,** Max Planck Institute for Biophysical Chemistry, Am Fassberg 11, 37077 Göttingen, Germany*
*3 - **Institute for Organic and Biomolecular Chemistry,** University of Göttingen, Tammannstrasse 2, 37077 Göttingen, Germany*
*4 - **Electron Microscopy,** Max Planck Institute for Biophysical Chemistry, Am Fassberg 11, 37077 Göttingen, Germany*

***Correspondence to Adam Lange and Bert L. de Groot:** adla@nmr.mpibpc.mpg.de; bgroot@gwdg.de*
http://dx.doi.org/10.1016/j.jmb.2013.10.020
Edited by D. P. Raleigh

Abstract

Recently, several short peptides have been shown to self-assemble into amyloid fibrils with generic cross-β spines, so-called steric zippers, suggesting common underlying structural features and aggregation mechanisms. Understanding these mechanisms is a prerequisite for designing fibril-binding compounds and inhibitors of fibril formation. The hexapeptide VEALYL, corresponding to the residues B12-17 of full-length insulin, has been identified as one of these short segments. Here, we analyzed the structures of multiple, morphologically different (fibrillar, microcrystal-like, oligomeric) [^{13}C, ^{15}N]VEALYL samples by solid-state nuclear magnetic resonance complemented with results from molecular dynamics simulations. By performing NHHC/CHHC experiments, we could determine that the β-strands within a given sheet of the amyloid-like fibrils formed by the insulin hexapeptide VEALYL are stacked in an antiparallel manner, whereas the sheet-to-sheet packing arrangement was found to be parallel. Experimentally observed secondary chemical shifts for all aggregate forms, as well as ∅ and ψ backbone torsion angles calculated with TALOS, are indicative of β-strand conformation, consistent with the published crystal structure (PDB ID: 2OMQ). Thus, we could demonstrate that the structural features of all the observed VEALYL aggregates are in agreement with the previously observed homosteric zipper spine packing in the crystalline state, suggesting that several distinct aggregate morphologies share the same molecular architecture.

Introduction

The accumulation of β-sheet-rich amyloid aggregates via the fibrillogenic pathway is a complex process associated with cellular toxicity in a number of human protein misfolding disorders, such as Alzheimer's and Parkinson's diseases [1–7]. Amyloid deposits are characterized by the abundance of *in vitro* or *in vivo* elongated, unbranched structures with a highly regular, often twisted morphology [2,3,8,9,4,10–12]. These filaments can derive from a diversity of self-assembling proteins unrelated in sequence or structure. They bind the fluorescent dye molecules Thioflavin T and Congo red with high affinity [13] and are built up from a generic cross-β substructure as revealed by their X-ray diffraction patterns [14].

Recently, *in vitro* studies have confirmed that many different polypeptide chains form filamentous aggregates with common physicochemical properties. Nevertheless, experimental characterization of amyloidogenic proteins has led to the discovery of a strong polydispersity. In particular, the early kinetic intermediates and metastable states are highly polymorphic and possess a large structural variability [3,15]. Among different aggregation states nonfibrillar oligomeric precursors, protofibrils and circular species have been identified [16,15,4,12].

Several studies have documented that short model peptides can convert into amyloid-like fibrils

and microcrystalline aggregates, or often both, under similar conditions in solution [17–22]. More importantly, the suggested principle structural similarities of microcrystalline and fibrillar assembly states offer an attractive opportunity to investigate general architectural features of protein aggregates, such as the cross-β spine and putative steric zipper sheet interfaces [18,8,20]. Therefore, the question remains to be answered to what extent fibrils and crystals differ in their structural organization.

Molecular polymorphism has been confirmed to be inherently present in amyloid fibrillogenesis [8,23,24], where differences are discussed to arise from either the supramolecular organization, that is, the specific association and packing mode of structural subunits (i.e., protofilaments, β-sheet layers) [25] and/or distinct forms of molecular conformations [21,20,19]. Hence, the elucidation of individual structural polymorphs on an atomic level is challenging and the conclusions drawn so far are still controversial [26–28]. Obtaining structural constraints for models of full-length amyloid peptides and proteins beyond the molecular level proves to be a major task and requires considerable effort in designing suitable experimental protocols and the use of state-of-the-art instrumentation [9,29,30,10,11,31].

In recent crystallographic studies on several fibril-forming peptides derived from known amyloidogenic proteins, structural models of commonly organized cross-β spines have been revealed [32,18,25]. These atomic-resolution structures demonstrate how the pairing of two elongated β-sheets of extended peptide strands leads to a tight and dry interface by a complementary interdigitation of residue side chains. This basic steric zipper motif can be classified into several symmetry groups composed of β-sheet arrays with distinct orientational arrangements of strands and sheets [18,33].

One of the sequences investigated in this context is the hexapeptide VEALYL, a derivative of residues 12–17 from the B chain of insulin [18,17,33]. The recently resolved three-dimensional crystal structure of VEALYL reveals a class 7 zipper, characterized by a face-to-back packing of the β-sheets, and antiparallel stacked strands within the sheets [18]. The VEALYL segment is proposed to play an important role in full-length insulin misfolding [34,35,18,36] and to participate in the β-strand core region of mature insulin fibrils [37,38].

Here, we analyzed the structures of different aggregation forms (fibrillar, microcrystal-like, oligomeric aggregates) of the VEALYL steric zipper peptide by solid-state nuclear magnetic resonance (ssNMR). To complement the discussion of the experimentally observed polymorphic peptide aggregates and the appearance of multiple resonance sets in the ssNMR spectra with additional insight at an atomic scale, we carried out a series of molecular dynamics (MD) simulations of VEALYL β-sheet model constructs.

Results

The fibrillar conformation of VEALYL corresponds to the proposed crystal structure

To elucidate the VEALYL structure in the fibrillar aggregation state, we applied two-dimensional magic angle spinning (MAS) ssNMR spectroscopy on partially labeled [u-^{13}C, ^{15}N-VEA]-[^{15}N-L]-[u-^{13}C, ^{15}N-Y]-L and [u-^{13}C, ^{15}N-VEALY]-L samples obtained from exactly the same fibrillization assay conditions, in the following named f1 and f2, respectively.

Electron micrographs of both fibrillized samples (Fig. 1a) show extended, unbranched, and twisted fibrils with diameters 20–40 nm for f1 and 10–20 nm for f2 fibrils. Likewise, the cross-over distance for f1 fibrils is much larger with an average of 330 nm compared to 80–90 nm for f2 fibrils. Despite the observation of macromolecular polymorphism between these fibrillar samples, the resulting two-dimensional proton-driven spin diffusion (PDSD) spectra show an overall comparable peak pattern (Fig. S1), indicative of similar structural features on the atomic level. Most noticeably, differences occur in the N-terminal valine C$^{\gamma}$ region. Surprisingly, at least two valine spin systems are observed in both the f1 and f2 samples, although the peptide contains only one valine residue, V1. Considering the line widths of the other resonances, the observed peak patterns suggest the presence of at least two different major and further minor resonance sets. Due to the low signal-to-noise ratio of the minor sets, an unambiguous sequential assignment of all the different sets was not feasible. However, we unambiguously assigned the main spin systems with highest intensity as illustrated in Fig. S2.

An analysis of the PDSD spectra with respect to secondary structure (Fig. 1c–e) shows that all residues adopt β-strand conformation in agreement with the crystal structure [18]. Additionally, for V1 and Y5 resonance sets with random-coil propensity observed, but since this does not hold for the remaining residues, a complete VEALYL random-coil conformation can be excluded. Especially in the case of V1, these resonances may result from an N-terminal loose packing.

To obtain long-range distance information, we conducted NHHC and CHHC experiments that indirectly probe ^{1}H–^{1}H through-space proximities via highly resolved rare spins (Fig. 1b and Fig. S3), such as ^{13}C and ^{15}N [39,40]. An overlay of an NHHC spectrum of the f2 sample with an NCOCX spectrum that exhibits sequential correlations between residues *i* and *i* – 1 reveals a high degree of similarity. This is due to a close proximity of the ^{1}HNi-^{1}HAi-1 spin pairs, as found in a β-strand conformation. An analysis of the PDSD spectra with regard to secondary structure propensity (Fig. 1c–e) shows that all residues adopt

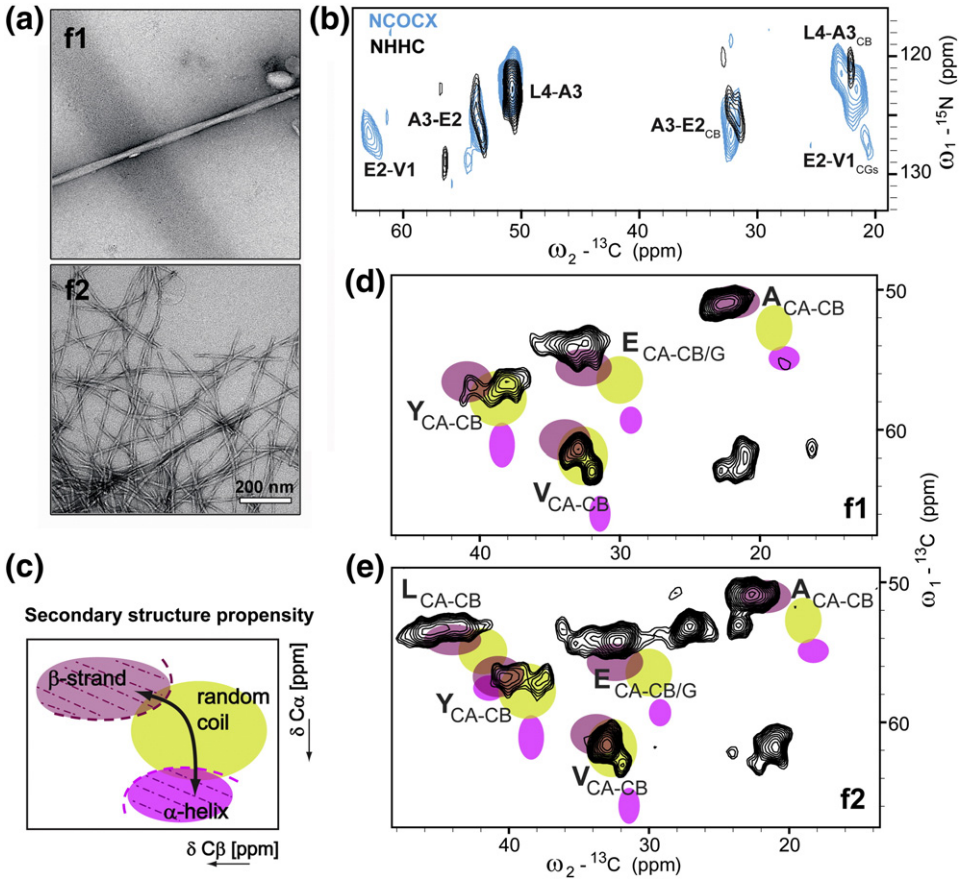

Fig. 1. VEALYL fibrils show β-strand propensity. (a) Electron micrographs of partially labeled [u-^{13}C,^{15}N-VEA]-[^{15}N-L]-[u-^{13}C,^{15}N-Y]-L and [u-^{13}C,^{15}N-VEALY]-L aggregated samples (f1 and f2, respectively). The scale bar represents 200 nm. (b) Overlay of NCOCX (blue) and NHHC (black; 0.3 ms of ^{1}H–^{1}H mixing) experiments recorded on the f1 sample. NHHC signals match the *i* to *i* – 1 signals perfectly due to a close proximity of the ^{1}HNi-^{1}HAi-1 spins, indicative of β-strand conformation. (c–e) Qualitative secondary structure prediction [42]. A small C^{β} and a large C^{α} chemical shifts are suggestive of α-helical conformation (purple). Vice versa, a large C^{β} shift and a small C^{α} shift indicate β-strand conformation (pink) (c). Spectra recorded with PDSD experiments (^{13}C–^{13}C mixing time of 20 ms). Resonances of both f1 (d) and f2 (e) fibrils show clear β-strand propensity. In addition for V and Y, a further resonance set in random-coil conformation is observed. All experiments were recorded on a 600-MHz spectrometer, at a spinning frequency of 11 kHz and a sample temperature of ~280 K. Further experimental details are given in Supplementary Information.

β-strand conformation, consistent with the crystal structure [18].

To determine the supramolecular arrangement of VEALYL molecules within the β-sheets, we performed CHHC experiments on both f1 and f2 samples and compared the results with the published crystal structure (PDB ID: 2OMQ; Fig. 2). The CHHC spectra were recorded with a ^{1}H–^{1}H mixing time of 300 μs such that distances up to a maximum of 3.5 Å are expected to result in strong cross-peaks. Different supramolecular arrangements were generated on the basis of the monomeric crystal structure, comparing observed and expected correlations. The most relevant distances are summarized in Table 1.

In both fibrillar samples, an E2-Y5 contact (Fig. 2a) that can only be explained by an antiparallel stacking of monomers is observed—corroborating the arrangement seen in the crystal structure (Fig. 2b). Additionally, we observed in the f2 fibrils a contact between the side chains of the labeled residue L4 and V1, in line with a parallel arrangement of laterally adjacent β-sheets (Fig. 2d and Table 1). This result corroborates a dry, class 7 steric zipper interface between pairs of β-sheets and proves that VEALYL fibrils share the same supramolecular arrangement as previously observed in the crystal structure.

VEALYL peptide solutions yield polymorphic aggregate structures that can interconvert

The partially labeled [u-^{13}C,^{15}N-VEA]-[^{15}N-L]-[u-^{13}C,^{15}N-Y]-L monomers were initially solubilized in polymerization buffer for fibril assembly and subsequently split into two parts to ensure proper

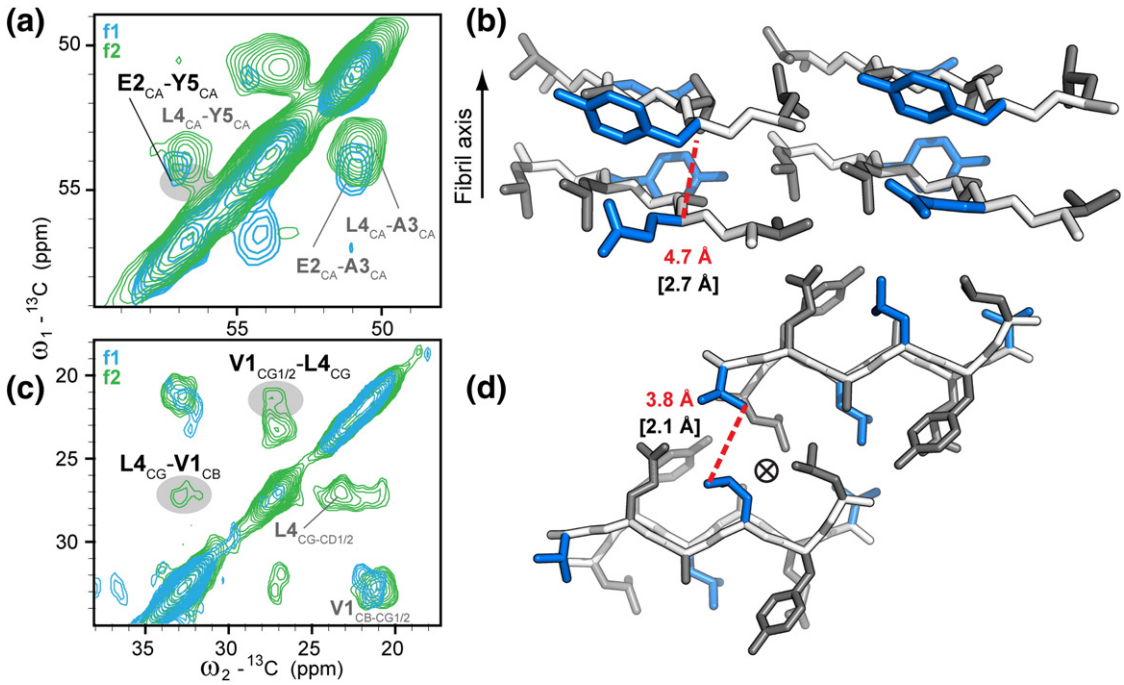

Fig. 2. Monomeric alignment within VEALYL fibrils. (a and c) Overlay of CHHC spectra (0.3 ms of ^{1}H–^{1}H mixing according to distances up to 3.5 Å) recorded on f1 (blue) and f2 (green) samples. (b and d) Distance measurements based on the crystal structure (PDB ID: 2OMQ). In both samples, E2-Y5 contacts (a) that are expected in an antiparallel stacking as in the crystal structure (b) are observed. In f2, the side chains of L4 (labeled in preparation f2) and V2 are in contact with V1 of another molecule, (c) which is in line with the parallel steric zipper arrangement of adjacent β-sheets (d). Spectra were recorded on a 600-MHz spectrometer, at a spinning frequency of 11 kHz and a sample temperature of ~280 K. Further experimental details are given in Supplementary Information.

agitation. Surprisingly, after incubation, only one of the two solution batches yielded fibrils (f1; Fig. 1a). Electron micrographs of the other preparation show a mixture of fibrils and microcrystalline-like aggregates (m1; Fig. 3a). To validate our finding that initially monomeric peptide solutions can result in different aggregation forms under the same treatment after being split in two batches, we repeated the procedure for the [u-^{13}C, ^{15}N-VEALY]-L-labeled monomers. The one solution part yielded sample f2, the other preparation an amorphous precipitate (p2; Fig. 3b). Astonishingly, when comparing the PDSD spectra (Fig. 3c), the resonances of all four samples f1, m1, f2, and p2 superimpose very well, indicating a common core structure and a conserved supramolecular arrangement. Even the different major resonance sets found for the fibrillar forms seem to be conserved between the different species, indicated by similar peak patterns. The polymorphism observed for the V1 C^{γ} region of sample f1 is observed in m1 as well, in contrast to f2 and p2. Similar to the fibrillar samples f1 and f2, β-strand propensity is also observed for all residues in m1 and p2 as well (Fig. 3d and e). Furthermore, V1 and Y5 exhibit additional resonances characteristic of random-coil conformation. From the fact that p2 shows spectral signatures comparable to the other samples, while no fibrillar or microcrystalline-like aggregate material could be detected by electron

Table 1. Distance information identifies monomeric alignment within VEALYL fibrils

Atoms	Intrastrand distance (Å)	Intrasheet distance (Å)		Intersheet distance (Å)	
		Parallel	Antiparallel	Parallel	Antiparallel
E2 H^{α}-Y5 H^{α}	10.4	11.5	2.7	13.7	10.6
E2 C^{α}-Y5 C^{α}	10.3	10.8	4.7	13.7	10.8
V1 H^{γ}-L4 H^{δ}	8.4	10.3	7.3	2.1	6.9
V1 C^{γ}-L4 C^{δ}	9.3	11.6	8.1	3.8	8.2

Based on the crystal structure (PDB ID: 2OMQ), different fibril alignments were generated to measure E2-Y5 and V1-L4 distances. The experimental data are in agreement with the crystal structure.

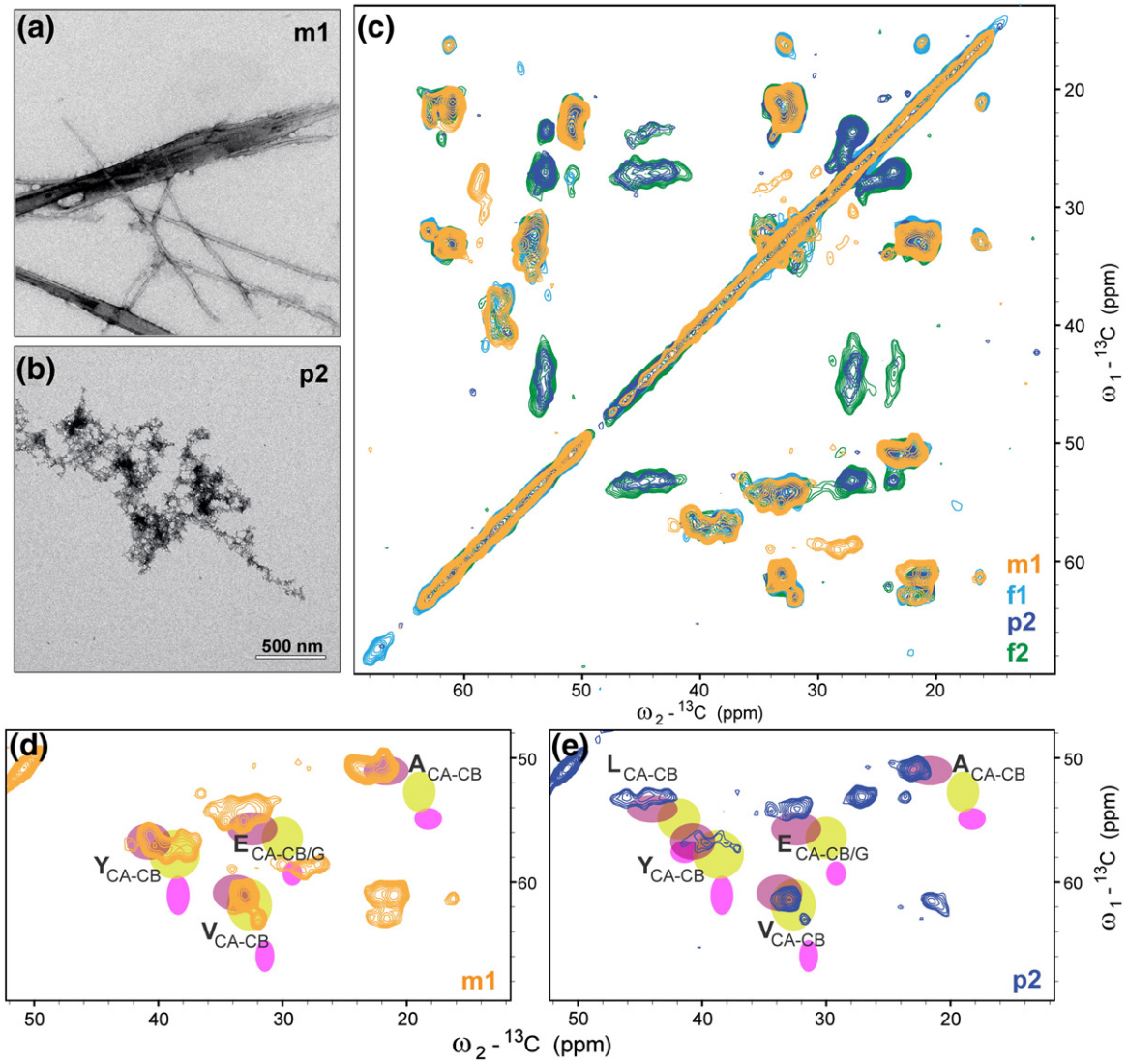

Fig. 3. Polymorphic VEALYL aggregates. (a) Electron micrographs show a mixture of fibrils and microcrystalline-like aggregates (m1) and (b) oligomeric assemblies (p2). (c) Aliphatic regions of PDSD spectra (^{13}C–^{13}C mixing time of 20 ms to obtain only intraresidue contacts) show a good overlay of the four different samples (f1, blue; m1, orange; f2, green; p2, dark blue). Note that L4 is only labeled in f2 and p2 samples. (d and e) Qualitative secondary structure prediction [42] for (d) m1 and (e) p2 aggregates. Spectra recorded with PDSD experiments (^{13}C–^{13}C mixing time of 20 ms). Resonances of both aggregation forms reveal β-strand propensity (purple). Additionally, V1 and Y5 exhibit a further resonance set corresponding to random-coil conformation (green). In the spectrum of m1, a set of E2 resonances with α-helical conformation (pink) is observed. Spectra were recorded on a 600-MHz spectrometer, at a spinning frequency of 11 kHz and a sample temperature of ~280 K. Further experimental details are given in Supplementary Information.

microscopy (EM), we conclude that p2 may be an oligomeric aggregation state. Within m1, a second set of E2 appears in an α-helical conformation. Analyzing the carbonyl/carboxyl region of the spectrum of m1 (Fig. S4, orange spectrum) shows that the E2, which is in α-helical conformation, is likely protonated at the side-chain carboxyl group, in agreement with what is observed for the E2 in β-strand conformation in this and the other samples. Additionally, very strong C^{δ}–C^{α}/C^{β}/C^{γ} correlations are observed for an unprotonated, that is, charged, E2 also in β-strand conformation. These correlations are absent in the spectra of the f1, f2, and p2 samples, indicating that no unprotonated E2 is present in these samples.

We sought to investigate the aggregation mechanism further and traced the assembly of unlabeled VEALYL monomers by EM over the course of 48 h using the same assay conditions as before (Fig. 4).

After dissolving the peptide in buffer and 1 h of incubation, globular structures and oligomeric

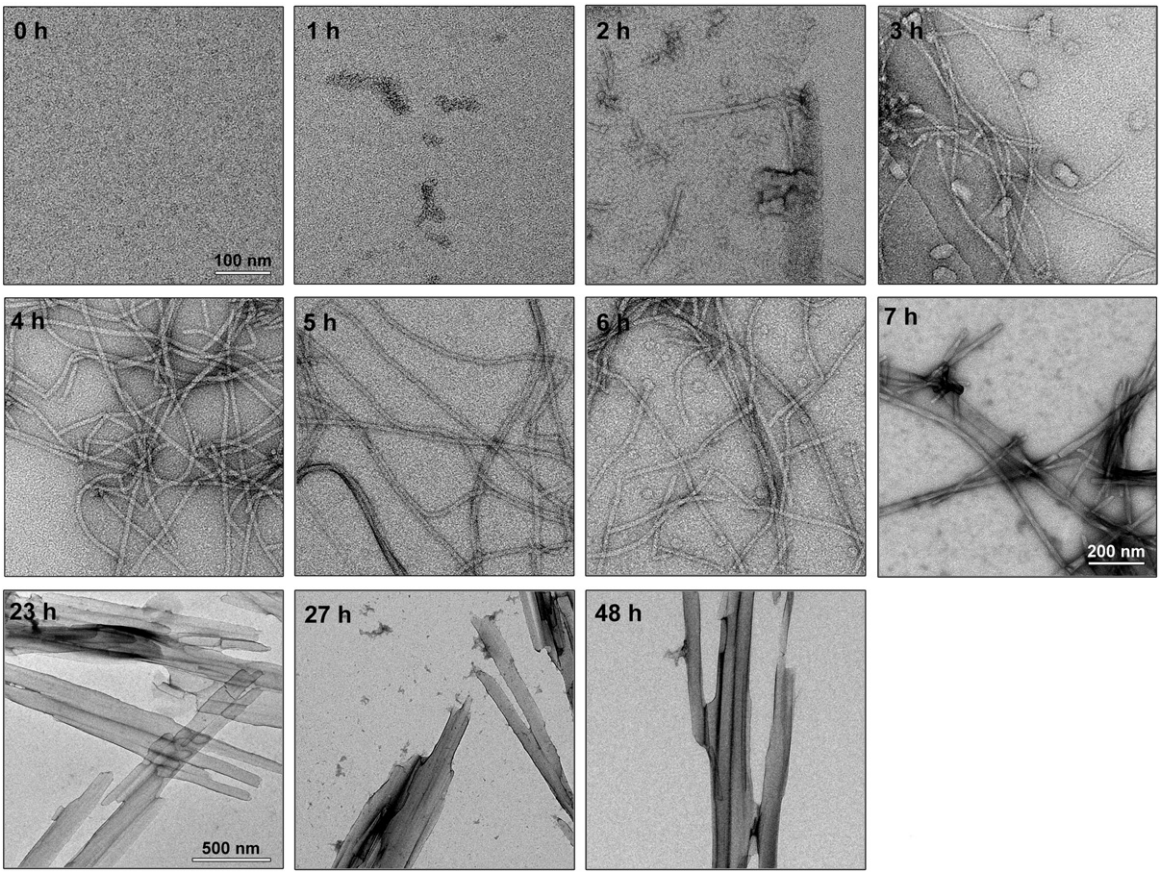

Fig. 4. Electron micrographs depicting a time trace of the assembly of unlabeled VEALYL peptides. Note that, in later aggregation stages, fibrillar aggregates turn over into microcrystalline-like states. The scale bar represents 100 nm (0–6 h), 200 nm (7 h), and 500 nm (23–48 h).

aggregates become visible in the electron micrographs (Fig. 4). At 2 h of incubation, a homogeneous growth starting from small filaments toward long, thread-like aggregates with the typical appearance of twisted amyloid-like fibrils could be observed (Fig. 4). However, after nearly half a day of incubation, the initially abundant fibrils with a uniform width of ~16 nm disappeared. Instead, paracrystalline, plate-like aggregates of much larger dimensions (Fig. 4) were visible, as also found for sample m1 (Fig. 3c). However, in both cases, the aggregates did not show diffraction spots in EM. Nevertheless, their appearance suggests a microcrystal-like nature [19].

It is likely that a spontaneous conversion from fibrillar to the observed microcrystalline-like aggregate forms took place during the sample incubation. To examine whether such structural transitions occurred also during the NMR measurements, we analyzed all investigated samples by EM after completion of the experiments. Overall, little changes of the macroscopic aggregation state could be detected. Interestingly, the EM image of sample m1 shown in Fig. S5 features the presence of at least one fibril that appears to grow from the tip of a microcrystal-like fragment, further highlighting the compatibility of the two aggregation forms. Similar observations have been made by Ivanova *et al*. and Sawaya *et al*. [17,18].

MD simulations support experimental findings on VEALYL aggregate conformations

As outlined above, the ssNMR spectra found for oligomeric, fibrillar, and microcrystalline-like aggregate samples growing under the same conditions (Fig. 3) did not exhibit any significant differences, suggesting a common arrangement of VEALYL peptide β-strands also consistent with the proposed homosteric zipper of class 7 [18,33]. Our initial structural model of a β-sheet construct was therefore based on the available atomic coordinates of the previously solved high-resolution structure of VEALYL peptide microcrystals. The EM images of fibrillar and non-fibrillar oligomeric samples (Figs. 1a and 3a and b) suggest aggregated structures with lateral extension of more than one pair of β-sheets. Therefore, we

chose to simulate models composed of multiple VEALYL peptide cross-β filaments (see Fig. 5 and Materials and Methods).

In addition and to address the question whether the observed macromolecular polymorphism could result from the sample preparation, we varied the initial protonation states of the peptides in the MD simulations (see Materials and Methods).

Structural stability and spontaneous twist of β-sheet model constructs

The initially planar β-sheet structures rapidly relax during the first 3 ns of unrestrained MD simulations (Fig. 6) and acquire a spontaneous, reproducible twist (Fig. 7a). Of all nine cross-β filaments in the construct, the central pair of β-sheets was most stable in terms of RMSD (Fig. 6b). Furthermore, the central cross-β filament was associated with the smallest twist angle (Fig. 7a), retaining an almost planar conformation for the setup with uncharged side chains but charged termini (zero net charge, mimicking VEALYL at pH 4). For the other systems with different protonation states, a notably larger average twist angle was observed (Fig. 7a).

While the fast structural reorganization results in the sampling of twisted β-sheet structures, significantly different from the planar crystal conformation, the changes of the individual peptide backbones remain relatively small (Fig. 7b). This can be seen by comparing the RMSD of the individual strands from the central cross-β filaments with respect to the starting (crystal) and final simulation structure (Fig. 7b).

Over the course of the simulations, the highly regular filament structures composed of stacked β-sheets with steric zipper interface were mostly retained, rendering the VEALYL constructs overall stable (see final structures in Fig. 6). As judged by the RMSD, the largest deviations from such ordered β-sheet conformations were observed for the model construct with net charge of +1 per VEALYL peptide (pH 2.5; Fig. 6a). This was due to noticeable fraying ends of the edge filaments, as well as an observed tendency of a wrapping instead of a twisting mode for the outer β-sheets (Fig. 6a). Interestingly, the

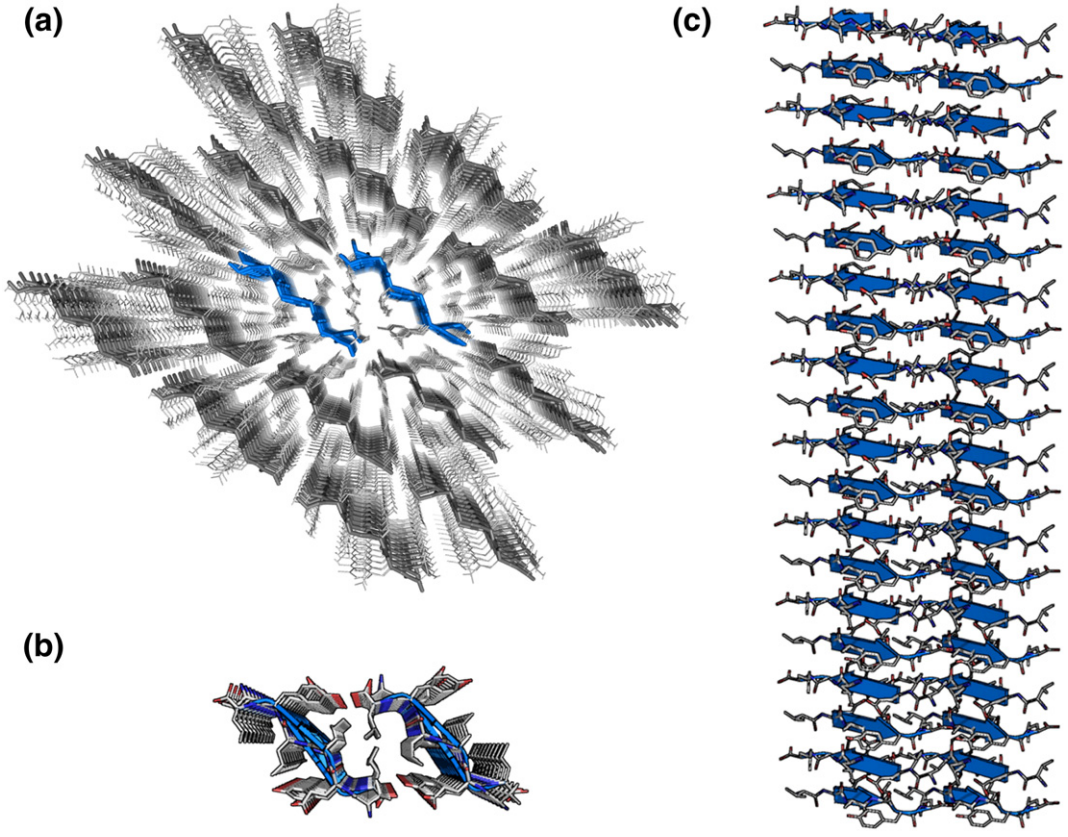

Fig. 5. Visualization of the VEALYL cross-β steric zipper model construct. (a) Stick representation of the VEALYL β-sheet structure model based on the available crystal structure coordinates (PDB ID: 2OMQ). The aggregate construct consists of nine steric zipper β-sheet pairs (1–9) with each sheet being composed of 20 strands. (b and c) A top and side view of the central steric zipper β-sheet filament is shown in cartoon representation highlighting the antiparallel strand orientation.

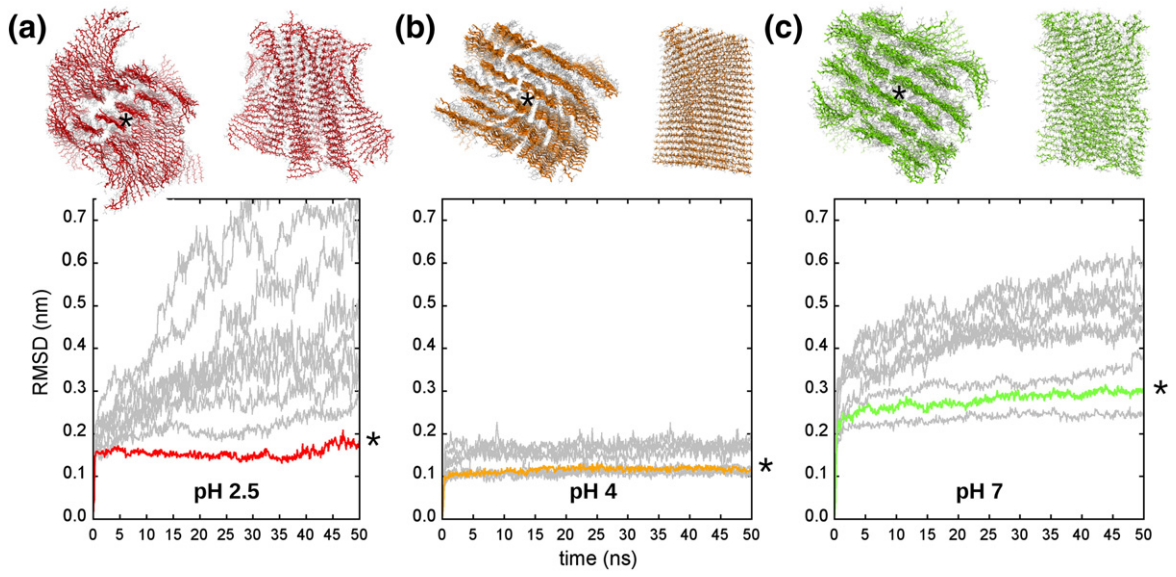

Fig. 6. Time evolution of the structural changes associated with the equilibration of the VEALYL cross-β model constructs. Top and side views of representative structures from the end of the trajectories (50 ns) are shown for the simulated array of β-sheet pairs with different protonation states: (a) pH 2.5, (b) pH 4, and (c) pH 7. The RMSD of the main chain and C^{β} atoms over time are shown for each of the nine cross-β filament structures with steric zipper interface, respectively. The RMSD curves of the central pair of β-sheets are marked by an asterisk.

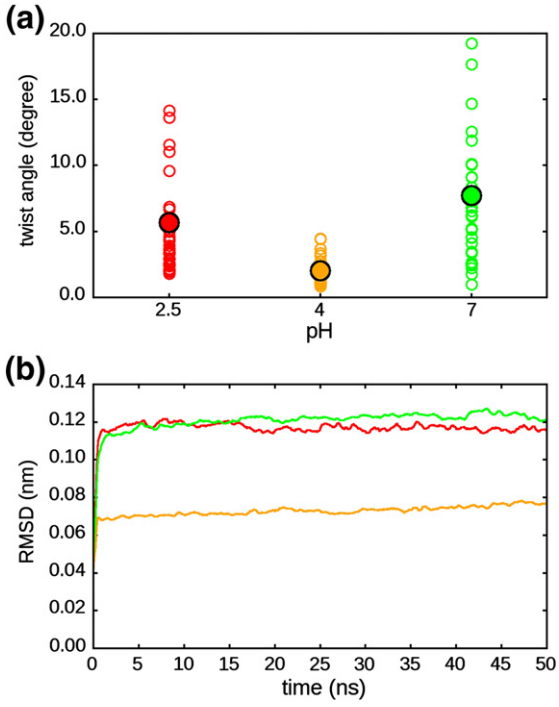

Fig. 7. Twist of VEALYL cross-β filaments. (a) Spontaneous twist of the central cross-β filament for three distinct VEALYL protonation states as obtained from the unrestrained MD simulations. The average twist angle of neighboring peptide strands are shown by large filled circles and individual values are shown by small open circles, respectively. (b) Average backbone atom RMSD of individual peptide structures from the central cross-β filament with respect to the crystal structure.

cross-β filaments were significantly less distorted and twisted as compared to the case of VEALYL with net charge of −1 (pH 7; Figs. 6c and 7a).

This suggests that electrostatic interactions involving the termini and side chains within the sheets, as well as intersheet packing interactions, significantly influence the structural stability and degree of twist.

Comparison of ssNMR chemical shift data of twisted and untwisted structures from MD simulations

In the free MD simulations, a spontaneous twisting of VEALYL cross-β filaments to a varying degree was observed. To examine the distinct conformational dependence and in order to investigate the effect of relaxation and twisting on the chemical shifts, we compared the experimentally measured resonance spectra with the predicted C^{α} and C^{β} cross-peaks calculated from various VEALYL β-sheet model construct simulations (Fig. 8 and Figs. S6 and S7; see Materials and Methods).

The C^{α} and C^{β} chemical shifts were predicted based on three kinds of MD input conformations: (i) planar pairs of VEALYL β-sheets (common starting configuration for all simulations) whose crystal structure coordinates were energy minimized prior to analysis, mimicking the situation in a crystal at low temperatures. An ensemble of simulation snapshots from (ii) a run with positional restraints applied to enforce untwisted cross-β filament conformations and (iii) conformations of free, unrestrained MD simulations of the VEALYL β-sheet model constructs.

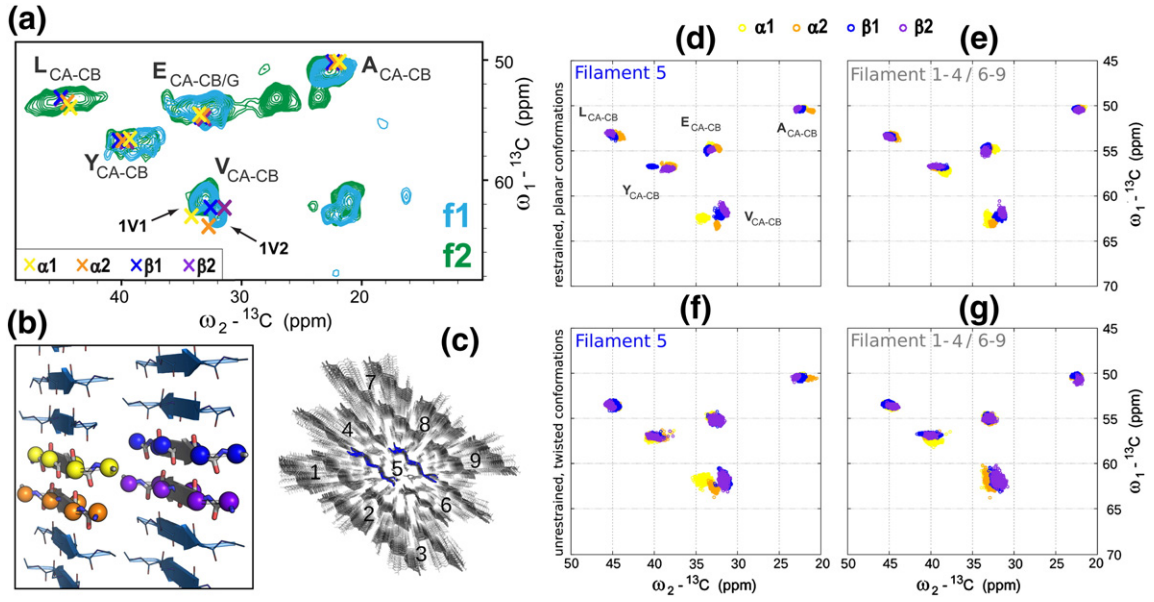

Fig. 8. Comparison of predicted chemical shift sets (MD) and experimentally measured fibrillar VEALYL aggregate conformations. (a) Chemical shift predictions calculated from energy-minimized steric zipper model structures are shown as crosses together with the experimentally measured ssNMR ^{13}C–^{13}C PDSD spectra of the fibrillar VEALYL samples (f1, blue; f2, green; see Materials and Methods). (b) The calculated C^{α} and C^{β} chemical shifts were assigned to four analysis sets (α1, α2, β1, and β2) according to the molecules in the asymmetric unit of the VEALYL crystal structure, that is, the arrangement of the pseudo-equivalent peptide conformations within the basic β-sandwich. For clarity, only the backbone atoms are shown. The C^{α} atoms of four neighboring peptides shown in sphere representation illustrate the specific packing symmetry classified as homosteric zipper class 7 (stacking pattern of strands and sheets in the steric zipper conformation) [33]. (c) In addition, the chemical shift sets of the central and the eight peripheral cross-β filaments from (c and d) position restraint, planar, and (e and f) unrestrained twisted model construct conformation ensembles are shown as open circles, respectively. As before, the different colors denote the four resonance sets.

The overlay of experimental PDSD spectra of fibrillar VEALYL samples with the predicted chemical shift averages calculated from planar pairs of VEALYL β-sheets (Fig. 8a) shows an agreement within the accuracy of the semi-empirical method implemented in the SHIFTX program [41] used to calculate them.

In accordance with the experimental cross-peaks, a prominent and characteristic splitting of the calculated chemical shift resonance sets for the N-terminal valine residue was found for the crystal structure conformation, as well as the position restrained and unrestrained MD structure ensembles (Fig. 8a and d–g).

The overall strongest resonance set splitting for all VEALYL residues was found in case of the energy-minimized structure (Fig. 8a) and the enforced, planar β-sheet conformations (Fig. 8d and e). However, the significant set splittings were found to vanish in the scenarios of spontaneously twisted structures for all but the N-terminal V1 residue (Fig. 8f and g). In addition, the comparison of the central (Fig. 8c, d, and f and Figs. S6a and S7a) with its surroundings, solvent-exposed cross-β filaments (Fig. 8c, e, and g and Figs. S6b and S7b), further highlights the dependence of β-sheet twist angle and the sampling of distinct C^{α} and C^{β} chemical shift sets, as well as their spectral width. These findings may explain the experimentally observed line broadening and resonance splittings. On the one hand, they are caused by the inherent steric zipper symmetry as found in the crystal structure, that is, the configuration of the asymmetric unit containing four pseudo-equivalent VEALYL molecules (Fig. 8b). On the other hand, the structural heterogeneity of differently twisted cross-β filaments can influence the range and features of the observed chemical shifts as well.

There was no apparent systematic difference across the ensemble of structures obtained from the calculations of chemical shifts for the three different protonation states in terms of the pattern and extent of resonance splitting (Figs. S6 and S7).

The site-specific secondary chemical shifts [42] agree qualitatively with the ones from the experimental spectra (data not shown). That is, on the one hand, secondary chemical shifts indicative of β-strand conformations are observed for almost all the sets of all the residues, as typical for fibrils. On the other hand, a prominent difference from this β-strand propensity was found in at least two of the resonance sets of the V residues; instead, more of a random-coil or an α-helical conformation was predicted (Fig. 1d and e and Fig. 8).

Discussion

Understanding the structural relationships of amyloid aggregate species from oligomeric intermediates through mature fibrils rests on the knowledge of their atomic configurations. Here, we have studied several different spontaneously *in vitro* aggregated forms of the short segment VEALYL from peptide hormone insulin. We utilized ssNMR for the structural elucidation of fibrillar, microcrystal-like, and oligomeric aggregates VEALYL peptide samples obtained from the same aggregation conditions. Irrespective of their characteristic morphological appearance in EM micrographs, comparable patterns of cross-peaks were observed in ssNMR spectra recorded on these samples, consistent with the principal arrangement of the peptide molecules in a class 7 steric zipper, as revealed in the crystal structure reported by Sawaya *et al*. [18].

Previous crystallography studies identified a characteristic cross-β structure with β-strands arranged in several possible steric zipper classes, showing that polymorphic samples can be explained by a variety of ways the peptides pack within the crystal [25,18,43,22] and by different crystal forms [19]. In the present study, we could exclude alternative packing modes for the observed VEALYL aggregates as demonstrated in Fig. 2 and Table 1. Moreover, the fibrillar VEALYL aggregates were found to form with steric zipper spine arrangement and thus confirm the close structural relationship with the previously observed homosteric zipper packing in the crystalline state [18]. Although fundamental structural similarities between amyloid-like peptide fibrils and crystals have been discussed [28,19,20,18,44,45], there are also important differences giving rise to distinct resonance sets [19,20,27]. A substantial increase in structural and dynamical complexity, both in local backbone conformations and in side-chain conformations, has been suggested for the fibrillar state [19,20,44,46].

Most importantly, we do not probe a scenario where multiple, laterally associated conformers form a structurally complex protofilament structure [28], as recently demonstrated for the amyloidogenic GNNQQNY peptide. However, to aid the interpretation on the molecular level, we built models of VEALYL cross-β filaments on the basis of the available crystal structure to examine in atomic detail the structural differences resulting from the supramolecular arrangement and their effect on the chemical shifts. Following the approach as discussed by Nielsen *et al*., we used the symmetry information of the basic steric zipper packing motif to calculate multiple resonance sets corresponding to the number of non-equivalent copies of VEALYL peptides found in the asymmetric unit of the crystal structure [27]. The chemical shifts calculated from structure ensembles obtained by all-atom MD simulations were found to be consistent with the expected symmetry-induced resonance splitting of the basic steric zipper packing model, as well as with all of the available experimental resonance data (Fig. 8). Overall, the degree of β-sheet twist did affect the predicted chemical shift sets of the VEALYL residues, as suggested by the analysis of the differently twisted cross-β filament conformations (Fig. 8d–g and Figs. S6 and S7). In particular, the central cross-β filament, which retained an almost planar β-sheet conformation, even in the unrestrained simulations, showed several well-defined resonance sets.

The found resonance set splittings for V1 could in part be explained by the supramolecular arrangement of the VEALYL molecules in a specific homosteric zipper configuration [18,33] as shown by our chemical shift predictions. Therefore, we conclude that a combination of β-sheet twist and different steric environments imposed by the zipper spine symmetry is likely to give rise to the measured pattern of the cross-peaks. An insufficient sampling of all the rotameric states in the MD simulations may explain why the predicted shift sets cannot fully account for the experimentally observed spectral width and shape of the cross-peaks.

A spontaneous twisting of the β-sheet constructs was observed in the simulations, although the molecular structure of the peptide monomers was similar (RMSD) between twisted and untwisted β-sheet conformations. It has been argued that the long-range twist and, thus, the repeat length of the filamentous aggregates are determined by small local changes in the interstrand angle of even a fraction of a degree [47]. Here, the smallest observed twist between the β-strands in the simulations (about 2–3° in pH 4 setup) corresponds to ~120–180 peptide layers (56–85 nm) per full turn considering an interstrand spacing of 4.7 Å. The experimental helical pitch values, as observed from the apparent twist periodicity of the fibrillar samples in the EM images, imply a larger number of peptide molecule layers per turn cross-over distance and a smaller interstrand twist angle. However, the values are of the same order of magnitude and the deviation results most likely from the finite-sized model construct structures in the simulations. The degree of interstrand twist in the cross-β filaments was found to differ depending on the steric environment, that is, the presence of additional, laterally, or terminally packed β-sheets, as well as the protonation state of the peptides, consistent with previous theoretical experimental work [48–51,47,31]. Along these lines, cross-β filaments with varied width and thus varying degree of intrasheet twist might therefore provide a rationale for the morphological variations between the two states of ribbon-like fibrils observed by EM in the present study and elsewhere. Moreover, such a scenario would thus be also consistent with (few) significant conformations found by means of NMR [28,19]. In addition to fibrillar aggregates composed

of uniformly packed cross-β filaments with common substructure, fibrils with "composite" cross-β building blocks [28], hierarchically assembled β-sheet arrays [31], and the possible supercoiling to multiple protofilament [47] are discussed in the literature.

As seen from the time trace of EM micrographs obtained from the incubated VEALYL peptide solution (Fig. 4), a homogeneous growth of filamentous structures was followed up by the appearance of microcrystal-like aggregate morphologies. While the exact kinetic pathway between fibrillar and microcrystalline state remains elusive, previous studies [45,46] of the GNNQQNY peptide—one of various short sequences that has been found to self-assemble into β-sheet-rich amyloid-like fibrils and microcrystals [17,18,51]—have correlated side-chain rearrangements with the transition from fibrils to crystals. Previous reports also highlight that fibrils are distinguished from their crystalline counterparts by an increased complexity, both structurally and dynamically [28]. However, recently, it has been proposed that the conversion from fibrillar to crystalline aggregates can essentially be described by a twisting transition of the β-sheet structures [51]. The generic driving force for this transition may be the greater thermodynamic stability of the microcrystalline state as indicated by a shift in the equilibrium between the peptide in solution and in microcrystals stronger than that in the corresponding monomer or fibril equilibrium [51], although the robustness of the aggregation process, that is, the dependence of initial peptide concentrations, is still under debate [46,28,19,20]. The results from the current work suggest that distinct aggregation states associated with different interstrand twist angles are all compatible with the same ssNMR resonance pattern. For the interconversion of fibrillar and crystalline states to occur, a transition without a major change in the β-sheet architecture therefore seems likely, for example, via the successive lateral association of initially twisted, fiber-like cross-β filaments toward larger, microcrystalline peptide arrays with planar β-sandwich conformations [46].

Furthermore, the oligomeric aggregates observed in the p2 sample were found to be distinct in morphology from the appearance of fibrillar and microcrystal-like aggregates as characterized by EM. As reflected by their similar NMR signals, oligomeric aggregates and fibrils/microcrystal-like aggregates share the same structural features, indicative of a common supramolecular organization in the same steric zipper motif/cross-β architecture. Given that the oligomeric aggregates were found to be stable over a period of more than 12 months points to aggregate species off-pathway to fibrils [52–54]. Note that phosphate buffer was used for peptide polymerization (see Materials and Methods), which sometimes leads to artificial precipitates in the EM analysis, rendering it difficult to unambiguously determine the nature of this aggregation state. It is, however, tempting to speculate that the oligomeric aggregates are similar to the ones previously reported for Aβ [52,53]. Such oligomer structures were found to potentially exhibit long-range disorder, resulting from a restricted sheet-to-sheet contact surface [55,15,54]. As may be the case for the p2 aggregates, these oligomers consists of identical basic units of largely invariant ordered monomer conformations and thus may also have a very similar structural organization to those of the fibrillar and crystalline phases [54,52]. Interestingly, in our MD simulations of the finite-sized VEALYL β-sheet model constructs, the edges of the outer β-sheet filament pairs were found to wrap at high twist angles in order to create contact, and thus binding energy, as well as optimized hydrogen bond interactions within the β-sheets [56,52]. This finding suggests that oligomers with cross-β structure are likely stabilized by/composed of multiple protofilaments that twist around an internal helical axes [31].

Altogether, our results support the notion that the steric zipper is the basic motif of β-strand arrangement in various states of self-assembled VEALYL peptide aggregates with distinct morphology, thus providing a molecular picture for the generic cross-β structure of amyloids and amyloid-like assemblies [18,21,22,57].

Conclusion

Short amyloid-like peptides have been established as very effective model systems in probing multiple relevant states on the complex aggregation landscape with a variety of experimental and computational techniques [58,57,52,54,50]. Our study of spontaneously aggregated VEALYL peptide solutions revealed a principal structural interrelationship of several, different aggregate morphologies obtained from a single aggregation protocol. The fibrillar VEALYL conformation displays a steric zipper peptide arrangement similar to the proposed crystal structure, namely, a parallel-layered, antiparallel β-sheet that extends perpendicular to the fibril axis. In addition, oligomeric and microcrystal-like VEALYL peptide aggregates were shown to share the same basic molecular architecture. Our findings from ssNMR measurements were complemented with atomistic simulations showing that the different packing environments of the amino acids in the specific homosteric zipper configuration can in part explain the multiple resonance sets observed experimentally.

We envision that our efforts in elucidating the molecular details of the fibrillar aggregates will spark further progress in the structural characterization of these potentially toxic species. Improving our understanding of the multitude of aggregate states could eventually lead up to the design of a comprehensive inhibitory strategy involving conformation specific targets [22].

Materials and Methods

Peptide synthesis

Solvents were of the highest grade available. The different VEALYL peptides were synthesized via manual Fmoc solid-phase synthesis on preloaded Fmoc-Leu Wang resin. Further details are available in Supplementary Information.

Aggregation assay

Polymerization buffer contained 50 mM phosphate and 150 mM NaCl (pH 2.5). Aggregation was initiated by incubating soluble monomeric VEALYL peptide, typically in the concentration range 14 mM in the presence of 0.02% NaN_3 for ~3 weeks at 310 K and agitation of 250 rpm. After incubation, the solution was centrifuged at 40,000*g* for 30 min. The morphology of the aggregates was analyzed by EM.

Electron microscopy

The protein samples in phosphate buffer were bound to a glow-discharged carbon coil covered grid, washed twice with H_2O, and negatively stained with 1% uranyl acetate. The specimens were evaluated with a CM120 transmission electron microscope (FEI, Eindhoven, The Netherlands).

ssNMR experiments

Two-dimensional ssNMR experiments were conducted using a 4-mm triple-resonance (^1H,^{13}C,^{15}N) MAS probe at a static magnetic field of 14.1 T corresponding to 600 MHz ^1H resonance frequency (Bruker Biospin, Karlsruhe, Germany). ^{13}C and ^{15}N chemical shifts were calibrated either with Adamantane as an external reference or with DSS as an internal reference [59]. In the latter case, the temperature-dependent position of the water proton resonance was used to measure the temperature inside the MAS rotor [60]. All experiments were recorded at a sample temperature of ~280 K and at a MAS frequency of 11 kHz. Typical proton field strength for 90° pulses and SPINAL-64 [61] high-power ^1H–^{13}C decoupling was 83 kHz. An initial ramped cross-polarization (CP) was used to transfer magnetization from ^1H to ^{13}C or ^{15}N with contact times between 600 and 1000 μs. ^{13}C–^{13}C transfer was achieved via PDSD [62] with mixing times of 20 and 150 ms to obtain intraresidue and sequential correlations, respectively. Sequential assignments were also obtained by means of NCACX and NCOCX experiments. ^{15}N-to-$^{13}C^{\alpha}$ transfer utilized SPECIFIC-CP [63] for a contact time of 2–3 ms. In these experiments, PDSD or DARR [64] elements were used for 20 ms of homonuclear ^{13}C–^{13}C transfer. Additionally, CHHC [39] and NHHC experiments were recorded with short CP times of 100–200 μs and a ^1H–^1H mixing time of 300 μs. Interscan delays were set to 2 s. All NMR spectra were analyzed using Sparky version 3.100 (T. D. Goddard and D. G. Kneller, University of California). Further experimental details are given in the SI (Table S1).

MD simulations

Initial conformations, molecular modeling, and simulated systems

In order to probe the structural stability and estimate the chemical shifts of fibrillar and microcrystalline-like VEALYL peptide aggregates, we have performed MD simulations of cross-β model constructs (see Fig. 5).

Simulated systems

An overview of the simulated cross-β aggregate model constructs and the respective simulation lengths is given in Table S2. The simulations were categorized according to the name of the peptide, the starting configuration, and the protonation state. To study the effect of pH, we simulated the model constructs with three different protonation states of the titratable groups of the VEALYL peptide.

For pH 2.5, the carboxyl groups of the peptides C-termini (COOH), as well as the glutamic acids (GluH), were assumed to be protonated according to experimental conditions in this study and the crystallization protocol [17,18]. For pH 4, the Glu residues were considered to be protonated, whereas for pH 7, they were not protonated and hence negatively charged.

Initial conformations

The atomic coordinates of the crystal structure PDB entry 2OMQ [18] were used to build the VEALYL peptide cross-β filament models. Further details on the creation of the model constructs are given in Supplementary Information.

Each construct was placed in a rectangular periodic box with adequate dimensions, such that the box edges were more than 2.5 nm away from the solute. Explicit hydrogen atoms were added to the structures. The protonation state for the different systems was established as discussed above (Table S2). Subsequently, all systems were solvated with explicit water molecules and counter-ions (Na^+, Cl^-) were added to yield an ionic strength (0.15 mM) according to the experimental conditions and to neutralize the net system charge.

After the system preparation, an energy minimization using steepest descent was performed. To relax the solvent configuration further, we carried out a 100-ps MD run with position restraints imposed on all the peptide heavy atoms (force constant of 1000 kJ/mol) for every system. An additional equilibration simulation step of 100 ps length was performed, whereby only the heavy atoms of the peptide backbone were restrained (force constant of 1000 kJ/mol). After this equilibration procedure, the systems were allowed to move without any restraining forces in one case and with continuously restrained backbone atoms in the other case (see Table S2).

Setup and parameter

All MD simulations were carried out using the GROMACS software package (version 4.5) [65], employing the CHARMM27 force field [66] (with backbone potential [CMAP] correction), GROMACS port provided by Bjelkmar

et al. [67], and the TIP3P water model. The following simulation input parameter was used: the van der Waals interactions were switched off between 1.0 and 1.2 nm and short-range electrostatic interactions were cut off at 1.2 nm. All simulations were carried out using periodic boundary conditions and the particle mesh Ewald [68,69] method. The electrostatic interactions with particle mesh Ewald were calculated at every step with a grid spacing of 0.12 nm. The relative tolerance at the cutoff was set to 10^{-6}, and electrostatic interactions for a distance smaller than the real-space cutoff were calculated explicitly. All peptide bonds were constrained with the P-Lincs algorithm [70]. Water molecules were constrained using Settle [71]. Virtual interaction sites of all the hydrogen atoms were introduced, thereby removing all internal vibrational degrees of freedoms [72]. The simulations were run using a 4-fs integration time step. Neighbor lists for non-bonded interactions were updated every 5 steps. The Berendsen coupling algorithm [73] was applied to keep the pressure constant by coupling the system to a pressure bath of 1 bar (τ = 1 ps). Velocity rescale [74] was applied for temperature coupling to a temperature bath of 310 K. Initial velocities were taken from a Maxwellian distribution at 310 K.

For molecular visualization, the PyMOL graphics program [75] was used.

Analysis details

Chemical shift predictions

The isotropic ^{13}C chemical shifts (C^{α},C^{β}) of the structures sampled from the MD trajectories were estimated using the SHIFTX [41] program. Samples for analysis were collected every 100 ps from each of the trajectories. For each sampled simulation snapshot, the predicted C^{α} and C^{β} chemical shifts were averaged across the four different sets of supramolecular conformations (α1, α2, β1, and β2; see Fig. 8b–g and Figs. S6 and S7) corresponding to the four molecules present in the asymmetric unit of the VEALYL crystal structure, respectively. The assignment to the respective sets according to the chain position and specific symmetry of the homosteric zipper class 7 yields a total of eight peptide chains per set and filament structure. In addition, the chemical shift sets for the central pair of β-sheets and the eight surrounding cross-β filaments were analyzed in two separate groups. In order to allow for a direct comparison between these two analysis groups in terms of number of molecules contained, for each of the individual calculations for the peripheral cross-β filaments sets, we drew eight molecules out of the total number of 64 structures randomly. The ^{13}C chemical shift sets for the crystalline reference were calculated accordingly based on the energy-minimized VEALYL cross-β filament model structure.

Twist angle

The twist angle was calculated between two successive intrastrand vectors joining the C^{α},2 and C^{α},5 atoms of the eight peptide pairs of the central cross-β filament. For the analysis, all possible neighboring intrasheet peptide pairs were considered, except from the two closest strands to the filament edge, respectively.

Supplementary data to this article can be found online at http://dx.doi.org/10.1016/j.jmb.2013.10.020.

Acknowledgment

We thank Brigitta Angerstein for expert technical assistance. This work was funded by the Max Planck Society and the Deutsche Forschungsgemeinschaft [Emmy Noether Fellowship to A.L. and Graduate School Spectroscopy and Dynamics of Molecular Coils and Aggregates (GRK782)]. There are no private sector financial conflicts of interest by the authors.

Received 3 May 2013;
Received in revised form 9 October 2013;
Accepted 15 October 2013
Available online 25 October 2013

Keywords:
chemical shift;
amyloid;
polymorphism;
molecular dynamics;
solid-state NMR

†D.M. and V.D. contributed equally to this work.

Abbreviations used:
MD, molecular dynamics; ssNMR, solid-state nuclear magnetic resonance; MAS, magic angle spinning; PDSD, proton-driven spin diffusion; EM, electron microscopy; CP, cross-polarization.

References

[1] Kelly JW. Mechanisms of amyloidogenesis. Nat Struct Mol Biol 2000;7:824–6.
[2] Dobson CM. Protein folding and misfolding. Nature 2003;426:884–90.
[3] Chiti F, Dobson CM. Protein misfolding, functional amyloid, and human disease. Annu Rev Biochem 2006;75:333–66.
[4] Tycko R. Solid-state NMR studies of amyloid fibril structure. Annu Rev Phys Chem 2011;62:279–99.
[5] del Amo JML, Schmidt M, Fink U, Dasari M, Faendrich M, Reif B. An asymmetric dimer as the basic subunit in Alzheimer's disease amyloid beta fibrils. Angew Chem Int Ed 2012;51:6136–9.
[6] Comellas G, Lemkau LR, Nieuwkoop AJ, Kloepper KD, Ladror DT, Ebisu R, et al. Structured regions of alpha-synuclein fibrils include the early-onset Parkinson's disease mutation sites. J Mol Biol 2011;411:881–95.

[7] Helmus JJ, Surewicz K, Nadaud PS, Surewicz WK, Jaroniec CP. Molecular conformation and dynamics of the y145stop variant of human prion protein. Proc Natl Acad Sci U S A 2008;105:6284–9.
[8] Petkova AT, Leapman RD, Guo Z, Yau W-M, Mattson MP, Tycko R. Self-propagating, molecular-level polymorphism in Alzheimer's beta-amyloid fibrils. Science 2005;307:262–5.
[9] Fändrich M. On the structural definition of amyloid fibrils and other polypeptide aggregates. Cell Mol Life Sci 2007;64:2066–78.
[10] Schneider R, Schumacher MC, Mueller H, Nand D, Klaukien V, Heise H, et al. Structural characterization of polyglutamine fibrils by solid-state NMR spectroscopy. J Mol Biol 2011;412:121–36.
[11] Daebel V, Chinnathambi S, Biernat J, Schwalbe M, Habenstein B, Loquet A, et al. beta-Sheet core of tau paired helical filaments revealed by solid-state NMR. J Am Chem Soc 2012;134:13982–9.
[12] Ferguson N, Becker J, Tidow H, Tremmel S, Sharpe TD, Krause G, et al. General structural motifs of amyloid protofilaments. Proc Natl Acad Sci U S A 2006;103:16248–53.
[13] Westermark G, Johnson K, Westermark P. Staining methods for identification of amyloid in tissue. Methods Enzymol 1999;309:3–25.
[14] Sunde M, Serpell LC, Bartlama M, Frasera PE, Pepysa MB, Blake CCF. Common core structure of amyloid fibrils by synchrotron X-ray diffraction. J Mol Biol 1997;273:729–39.
[15] Fändrich M. Oligomeric intermediates in amyloid formation: structure determination and mechanisms of toxicity. J Mol Biol 2012;421:427–40.
[16] Kayed R, Head E, Thompson JL, McIntire TM, Milton SC, Cotman CW, et al. Common structure of soluble amyloid oligomers implies common mechanism of pathogenesis. Science 2003;300:486–9.
[17] Ivanova MI, Thompson MJ, Eisenberg D. A systematic screen of beta-2 microglobulin and insulin for amyloid-like segments. Proc Natl Acad Sci U S A 2006;103:4079–82.
[18] Sawaya MR, Sambashivan S, Nelson R, Ivanova MI, Sievers SA, Apostol MI, et al. Atomic structures of amyloid cross-beta spines reveal varied steric zippers. Nature 2007;447:453–7.
[19] van der Wel PCA, Lewandowski JR, Griffin RG. Solid-state NMR study of amyloid nanocrystals and fibrils formed by the peptide GNNQQNY from yeast prion protein Sup35p. J Am Chem Soc 2007;129:5117–30.
[20] van der Wel PC, Lewandowski JR, Griffin RG. Structural characterization of GNNQQNY amyloid fibrils by magic angle spinning NMR. Biochemistry 2010;49:9457–69.
[21] Madine J, Jack E, Stockley PG, Radford SE, Serpell LC, Middleton DA. Structural insights into the polymorphism of amyloid-like fibrils formed by region 20–29 of amylin revealed by solid-state NMR and X-ray fiber diffraction. J Am Chem Soc 2008;130:14990–5001.
[22] Eisenberg D, Jucker M. The amyloid state of proteins in human diseases. Cell 2011;148:1188–203.
[23] Heise H, Hoyer W, Becker S, Andronesi OC, Riedel D, Baldus M. Molecular-level secondary structure, polymorphism, and dynamics of full-length alpha-synuclein fibrils studied by solid-state NMR. Proc Natl Acad Sci U S A 2005;102:15871–6.
[24] Meinhardt J, Sachse C, Hortschansky P, Grigorieff N, Faendrich M. Abeta(1–40) fibril polymorphism implies diverse interaction patterns in amyloid fibrils. J Mol Biol 2009;386:869–77.
[25] Wiltzius JJW, Landau M, Nelson R, Sawaya MR, Apostol MI, Goldschmidt L, et al. Molecular mechanisms for protein-encoded inheritance. Nat Struct Mol Biol 2009;16:973–8.
[26] Cheng H-M, Tsai TWT, Huang WYC, Lee H-K, Lian H-Y, Chou F-C, et al. Steric zipper formed by hydrophobic peptide fragment of syrian hamster prion protein. Biochemistry 2011;50:6815–23.
[27] Nielsen JT, Bjerring M, Jeppesen MD, Pedersen RO, Pedersen JM, Hein KL, et al. Unique identification of supramolecular structures in amyloid fibrils by solid-state NMR spectroscopy. Angew Chem Int Ed 2009;48:2118–21.
[28] Lewandowski JR, van der Wel PCA, Rigney M, Grigorieff N, Griffin RG. Structural complexity of a composite amyloid fibril. J Am Chem Soc 2011;133:14686–98.
[29] Wasmer C, Lange A, Melckebeke HV, Siemer A, Riek R, Meier B. Amyloid fibrils of the HET-s(218–289) prion form a beta-solenoid with a triangular hydrophobic core. Science 2008;319:1523–6.
[30] Lv G, Kumar A, Giller K, Orcellet ML, Riedel D, Fernandez CO, et al. Structural comparison of mouse and human alpha-synuclein amyloid fibrils by solid-state NMR. J Mol Biol 2012;420:99–111.
[31] Fitzpatrick AWP, Debelouchina GT, Bayro MJ, Clare DK, Caporini MA, Bajaj VS, et al. Atomic structure and hierarchical assembly of a cross-beta amyloid fibril. Proc Natl Acad Sci U S A 2013;110:5468–73.
[32] Nelson R, Sawaya MR, Balbirnie M, Madsen AO, Riekel C, Grothe R, et al. Structure of the cross-beta spine of amyloid-like fibrils. Nature 2005;435:773–8.
[33] Stroud JC. The zipper groups of the amyloid state of proteins. Acta Crystallogr Sect D Biol Crystallogr 2013;69:540–5.
[34] Gibson TJ, Murphy RM. Inhibition of insulin fibrillogenesis with targeted peptides. Protein Sci 2006;15:1133–41.
[35] Nielsen L, Khurana R, Coats A, Frokjaer S, Brange J, Vyas S, et al. Effect of environmental factors on the kinetics of insulin fibril formation: elucidation of the molecular mechanism. Biochemistry 2001;40:6036–46.
[36] Haas J, Vöhringer-Martinez E, Bögehold A, Matthes D, Hensen U, Pelah A, et al. Primary steps of ph-dependent insulin aggregation kinetics are governed by conformational flexibility. ChemBioChem 2009;10:1816–22.
[37] Tito P, Nettleton EJ, Robinson CV. Dissecting the hydrogen exchange properties of insulin under amyloid fibril forming conditions: a site-specific investigation by mass spectrometry. J Mol Biol 2000;303:267–78.
[38] Ivanova MI, Sievers SA, Sawaya MR, Wall JS, Eisenberg D. Molecular basis for insulin fibril assembly. Proc Natl Acad Sci U S A 2009;106:18990–5.
[39] Lange A, Luca S, Baldus M. Structural constraints from proton-mediated rare-spin correlation spectroscopy in rotating solids. J Am Chem Soc 2002;124:9704–5.
[40] Lange A, Seidel K, Verdier L, Luca S, Baldus M. Analysis of proton-proton transfer dynamics in rotating solids and their use for 3D structure determination. J Am Chem Soc 2003;125:12640–8.
[41] Neal S, Nip A, Zhang H, Wishart D. Rapid and accurate calculation of protein ^{1}H, ^{13}C and ^{15}N chemical shifts. J Biomol NMR 2003;26:215–40.
[42] Wang YJ, Jardetzky O. Probability-based protein secondary structure identification using combined NMR chemical-shift data. Protein Sci 2002;11:852–61.
[43] Colletier J-P, Laganowsky A, Landau M, Zhao M, Soriaga AB, Goldschmidt L, et al. Molecular basis for amyloid-beta polymorphism. Proc Natl Acad Sci U S A 2011;108:16938–43.
[44] Debelouchina GT, Bayro MJ, van der Wel PCA, Caporini MA, Barnes AB, Rosay M, et al. Dynamic nuclear polarization-enhanced solid-state NMR spectroscopy of GNNQQNY nanocrystals and amyloid fibrils. Phys Chem Chem Phys 2010;12:5911–9.

[45] Marshall K, Serpell L. Fibres, crystals and polymorphism: the structural promiscuity of amyloidogenic peptides. Soft Matter 2010;6:2110–4.
[46] Marshall KE, Hicks MR, Williams TL, Hoffmann SV, Rodger A, Dafforn TR, et al. Characterizing the assembly of the Sup35 yeast prion fragment, GNNQQNY: structural changes accompany a fiber-to-crystal switch. Biophys J 2010;98:330–8.
[47] Jimenez JL, Nettleton EJ, Bouchard M, Robinson CV, Dobson CM, Saibil HR. The protofilament structure of insulin amyloid fibrils. Proc Natl Acad Sci U S A 2002;99:9196–201.
[48] Esposito L, Pedone C, Vitagliano L. Molecular dynamics analyses of cross-beta-spine steric zipper models: beta-sheet twisting and aggregation. Proc Natl Acad Sci U S A 2006;103:11533–8.
[49] Buchete N-V, Hummer G. Structure and dynamics of parallel beta-sheets, hydrophobic core, and loops in Alzheimer's Abeta fibrils. Biophys J 2007;92:3032–9.
[50] Periole X, Rampioni A, Vendruscolo M, Mark A. Factors that affect the degree of twist in beta-sheet structures: a molecular dynamics simulation study of a cross-beta filament of the GNNQQNY peptide. J Phys Chem B 2009;113:1728–37.
[51] Knowles TP, De Simone A, Fitzpatrick AW, Baldwin A, Meehan S, Rajah L, et al. Twisting transition between crystalline and fibrillar phases of aggregated peptide. Phys Rev Lett 2012;109:158101.
[52] Stroud JC, Liu C, Teng PK, Eisenberg D. Toxic fibrillar oligomers of amyloid-beta have cross-beta structure. Proc Natl Acad Sci U S A 2012;109:7717–22.
[53] Wu J, Breydo L, Isas J, Lee J, Kuznetsov Y, Langen R, et al. Fibrillar oligomers nucleate the oligomerization of monomeric amyloid beta but do not seed fibril formation. J Biol Chem 2010;285:6071–9.
[54] Walsh P, Neudecker P, Sharpe S. Structural properties and dynamic behavior of nonfibrillar oligomers formed by PrP(106–126). J Am Chem Soc 2010;132:7684–95.
[55] Liu M, Sawaya P, Cheng J, Zheng J, Nowick JS, Eisenberg D. Characteristics of amyloid-related oligomers revealed by crystal structures of macrocyclic beta-sheet mimics. J Am Chem Soc 2011;133:6736–44.
[56] Wang J, Gülich S, Bradford C, Ramirez-Alvarado M, Regan L. A twisted four-sheeted model for an amyloid fibril. Structure 2005;13:1279–88.
[57] Matthes D, Gapsys V, de Groot BL. Driving forces and structural determinants of steric zipper peptide oligomer formation elucidated by atomistic simulations. J Mol Biol 2012;421:390–416.
[58] Jaroniec CP, MacPhee CE, Astrof NS, Dobson CM, Griffin RG. Molecular conformation of a peptide fragment of transthyretin in an amyloid fibril. Proc Natl Acad Sci U S A 2002;99:16748–53.
[59] Morcombe CR, Zilm KW. Chemical shift referencing in MAS solid state NMR. J Magn Reson 2003;162:479–86.
[60] Boeckmann A, Gardiennet C, Verel R, Hunkeler A, Loquet A, Pintacuda G, et al. Characterization of different water pools in solid-state NMR protein samples. J Biomol NMR 2009;45:319–27.
[61] Fung BM, Khitrin AK, Ermolaev K. An improved broadband decoupling sequence for liquid crystals and solids. J Magn Reson 2000;142:97–101.
[62] Szeverenyi NM, Sullivan MJ, Maciel GE. Observation of spin exchange by two-dimensional Fourier transform ^{13}C cross polarization-magic-angle spinning. J Magn Reson 1982;47:462–75.
[63] Baldus M, Petkova AT, Herzfeld J, Griffin RG. Cross polarization in the tilted frame: assignment and spectral simplification in heteronuclear spin systems. Mol Phys 1998;95:1197–207.
[64] Takegoshi K, Nakamura S, Terao T. ^{13}C–^{1}H dipolar-assisted rotational resonance in magic-angle spinning NMR. Chem Phys Lett 2001;344:631–7.
[65] Pronk S, Pall S, Schulz R, Larsson P, Bjelkmar P, Apostolov R, et al. GROMACS 4.5: a high-throughput and highly parallel open source molecular simulation toolkit. Bioinformatics 2013;29:845–54.
[66] Mackerell AD, Feig M, Brooks CL. Extending the treatment of backbone energetics in protein force fields: limitations of gas-phase quantum mechanics in reproducing protein conformational distributions in molecular dynamics simulations. J Comput Chem 2004;25:1400–15.
[67] Bjelkmar P, Larsson P, Cuendet MA, Hess B, Lindahl E. Implementation of the CHARMM force field in GROMACS: analysis of protein stability effects from correction maps, virtual interaction sites, and water models. J Chem Theory Comput 2010;6:459–66.
[68] Darden T, York D, Pedersen L. Particle mesh Ewald: an *n*-log(*n*) method for Ewald sums in large systems. J Chem Phys 1993;98:10089–92.
[69] Essmann U, Perera L, Berkowitz ML, Darden T, Lee H, Pedersen LG. A smooth particle mesh Ewald method. J Chem Phys 1995;103:8577–93.
[70] Hess B. P-Lincs: a parallel linear constraint solver for molecular simulation. J Chem Theory Comput 2008;4:116–22.
[71] Miyamoto S, Kollman PA. Settle: an analytical version of the shake and rattle algorithm for rigid water models. J Comput Chem 1992;13:952–62.
[72] Feenstra KA, Hess B, Berendsen HJC. Improving efficiency of large time-scale molecular dynamics simulations of hydrogen-rich systems. J Comput Chem 1999;20:786–98.
[73] Berendsen HJC, Postma JPM, van Gunsteren WF, DiNola A, Haak JR. Molecular dynamics with coupling to an external bath. J Chem Phys 1984;81:3684–90.
[74] Bussi G, Donadio D, Parrinello M. Canonical sampling through velocity rescaling. J Chem Phys 2007;126:014101.
[75] DeLano W. The PyMOL molecular graphics system. http://www.pymol.org; 2002.